Received: 15 February 2021 | Revised: 15 August 2021 | Accepted: 7 November 2021

DOI: 10.1002/mmce.22981

RESEARCH ARTICLE

INTERNATIONAL JOURNAL OF RF AND MICROWAVE COMPUTER-AIDED ENGINEERING WILEY

360° angular coverage pattern and polarization diversities wideband circularly polarized multiple input multiple output antennas

Prashant Chaudhary[1] | **Ashwani Kumar**[2,3] | **Pramod Kumar**[3] | **Kamlesh Patel**[1] | **Ravi Kumar Arya**[4] | **Anand Kumar Verma**[1]

[1]Electronic Science, University of Delhi South Campus, New Delhi, India

[2]School of Engineering, Jawaharlal Nehru University, New Delhi, India

[3]Sri Aurobindo College, University of Delhi, New Delhi, India

[4]Department of Electronics & Communication Engineering, National Institute of Technology Delhi, Delhi, India

Correspondence
Ashwani Kumar, School of Engineering, Jawaharlal Nehru University, New Delhi 110067, India.
Email: ashwanikumar7@yahoo.com

Abstract

This article presents a new design of six-element prism and eight-element cubic circularly polarized multiple input multiple output (MIMO) antennas exhibiting pattern and polarization diversity characteristics. The proposed antennas have 360° angular coverage. Each element of the MIMO antenna is radiating power in a different direction; antenna-1 radiates in −30°, antenna-2 radiates in 30°, antenna-3 radiates in 60°, and antenna-4 radiates in 120°. Antenna-5 radiates in 150°, antenna-6 radiates in −150°, antenna-7 radiates in −120°, and antenna-8 radiates in −60°.The radiation pattern can be directed in a specific direction by exciting the particular antenna element. It has wideband circular polarization in X-band (8.0–11.8 GHz). The proposed MIMO antenna element consists of pairs of mirrored monopole antennas facing each other are configured in the form of the prism and cube. The chance of mutual coupling is very high in both the configuration. A hollow copper cylinder is placed inside the prism and cube to reduce the mutual coupling. The isolation between the antennas is found better than −24 dB. The impedance matching bandwidth is 3.8 GHz (8–11.8 GHz), and the 3 dB axial ratio bandwidth is 2.69 GHz (8.01–10.7 GHz). The envelope correlation coefficient is less than 0.09, and total active reflection coefficient is less than −10 dB in a wide bandwidth. High isolation and uncorrelated radiation patterns between the adjacent elements make the proposed six-element and eight-element antenna a good candidate for massive MIMO antenna systems. The size of the antenna is 38.8 × 38.8 × 23 mm^3, and this compact MIMO antenna is useful for X-band communication.

KEYWORDS

antenna, circular polarization, MIMO, pattern diversity, polarization diversity and wideband

1 | INTRODUCTION

With tremendous demands of high-data rate in wireless communication, multiple input multiple output (MIMO) antenna gives the promising solution. MIMO antennas use different diversity techniques, that is, spatial diversity, pattern diversity, and polarization diversity to increase the throughput. In spatial diversity, antennas are spatially apart in space. In spatial diversity, parasitic structures,[1] a tree-like structure,[2] a metamaterial and

 © 2021 Wiley Periodicals LLC.

neutralization line,[3] a radial stub loaded resonator (RSLR),[4] and electromagnetic bandgap (EBG) structure placed between the radiating elements[5,6] are suggested to improve the isolation between the closely spaced antennas. In pattern diversity, the radiation pattern of antennas is directed in a different direction in space, whereas in polarization diversity, all the antennas in the MIMO system have different polarizations. Pattern diversity between the antennas is realized by using three different ways to reduce the mutual coupling between multiple antennas. In the first method, different modes of the patch antenna are used to generate diverse radiation patterns.[7] The second method is based on different antennas that radiate in different directions.[8]In contrast, different phases in the array antenna feed are used in the third method to achieve different radiation patterns.[9]

Several descriptions are presented to obtain the polarization diversity in linearly polarized antennas.[10–12] Inverted-cone monopole is used for the vertical polarization (VP), while the cross bow-tie dipole is used for the horizontal polarization (HP).[10] In Reference 11, a multiband and dual-polarized omnidirectional antenna design for VP and HP is suggested. The omnidirectional patterns of both VP and HP can also be achieved by cutting two orthogonal slots on the walls of a slender columnar cuboid,[12] while a reconfigurable polarization diversity by using PIN diode is presented in Reference 13. A circular polarization (CP) diversity cavity-backed SIW antenna is also presented in Reference 14 in which the sense of polarization is controlled with the diodes. Some recently reported research works in a planar configuration have both pattern and polarization diversity with wideband CP simultaneously.[15–17] In Reference 15, a wideband circularly polarized MIMO antenna with pattern and polarization diversity for 4G and 5G with integrated sub-6 5G and LTE band for the mobile handset is reported, while in Reference 16 the MIMO antenna with wideband CP in X-band with pattern and polarization diversity is suggested. In Reference 17, a three-element MIMO antenna with pattern and polarization diversity for WLAN application is proposed, while in Reference 18 a planar antenna with frequency reconfigurable dual-band MIMO antenna with pattern and polarization diversity is discussed for WiFi and WiMAX.

The massive MIMO antenna technique provides one of the most promising solutions to achieve high-data rates for the current wireless communication systems. This technique uses many independent antennas where each antenna's functioning can be controlled in the communication systems. By employing massive MIMO, the radiated energy can be focused on extreme sharpness for a tiny region of space by using the enormous number of independently controlled antennas.[7,19,20] In Reference 7, a three-port ring antenna with polarization and pattern diversity is suggested, and in Reference 19 8-antenna MIMO array using a balanced, open slot antenna element for 5G smartphones is indicated. Simultaneously, an inverted-F stub fed hybrid loop antenna for 5G sub-6 GHz massive MIMO enabled handsets with wideband is suggested.[20]

Recently, researchers have been working on 3D antenna structures in cube exhibiting linear polarization diversity. In Reference 21, an omnidirectional MIMO array antenna with pattern diversity is achieved by orthogonal pattern phase shift. Diversity antennas,[22] radiated slot placed at each face of cube excited by three identical port arranged in orthogonal fashion exhibiting pattern and polarization diversity. In Reference 23, a slotted hollow metallic cube is excited by the probe from the vertex, giving pattern reconfiguration by switching the shorted PIN diode. A ring-configuration can be used to get both pattern and polarization diversity.[24] MIMO cube is suggested in Reference 25, where dipole element placed at the edges exhibiting pattern and polarization diversity. Theoretical study on MIMO parameter is presented for dipole antennas arranged in the cube form in Reference 26 showing pattern and polarization diversity. Pattern control can be achieved in the reconfigurable ultrawideband antenna by switching the PIN diode.[27] Eight-port cylindrical dielectric resonator antenna (CDRA) are placed orthogonally to obtain multi-direction pattern diversity.[28] Electric dipole with metasurface placed on the hexagonal 3D shape structure[29] has pattern diversity. In Reference 30, a comparative study on the MIMO parameter envelope correlation coefficient is presented with earlier published works. Characterization of the antenna with multiple ports is suggested in Reference 31, and a new parameter called total active reflection coefficient (TARC) is introduced. CPW feed antenna for band-notched characteristic arranged in a cuboidal pattern to realize spatial diversity is presented in Reference 32. The above-suggested MIMO antennas[23–32] have a narrow bandwidth, and some of them do not have pattern and polarization diversity simultaneously.

In this work, we have designed a new wideband 3D circularly polarized prism and cubical MIMO antennas with six and eight elements having a pattern and polarization diversity with angular coverage in the whole 360^{o}angular span. All antenna elements are arranged so that their radiation patterns are directed in a specific direction. A hollow copper cylinder inside the prism and cube has been used to avoid the antenna's mutual coupling. The isolation between the antennas is better than −24 B, while for adjacent corner radiating elements, it is better than −17.5 dB.

The article is organized as followed: Section 2 presents the two-element MIMO antenna design. It also

verifies our suggested method for other frequency bands. Section 3 discusses the six-element prism-shaped MIMO antenna with pattern and polarization diversity. Section 4 presents the eight-element cube-shaped MIMO antenna. Section 5 discusses the MIMO characteristics of the cubic antenna. Finally, it concludes with some possible applications.

2 | TWO ELEMENT MIMO ANTENNA DESIGN

The presented six-element prism and eight-element cubic shaped structured MIMO antennas are designed systematically in two steps. Before the prism and cubic structure, the two-element mirrored MIMO antenna facing each other with wideband CP is developed, as shown in Figure 1. The antenna is designed on FR-4 substrate having a relative permittivity, $\varepsilon_r = 4.4$, loss tangent of 0.02 and h = 0.8 mm. This two-element MIMO antenna structure has both pattern and polarization diversity simultaneously. The design steps of this MIMO antenna are systematically presented in Figure 2, and its layout with detailed dimensions is shown in Figure 1. The frequency response of the two-element MIMO antenna is shown in Figure 3.

This two-element MIMO antenna is designed in systematic successive five steps, which are illustrated in Figure 2.The antenna design starts from a simple square patch which is step-1(antenna-1). The square patch dimensions can be obtained by using Equation (1), where

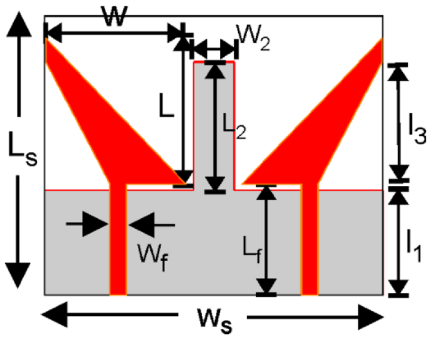

FIGURE 1 Two element MIMO antenna. MIMO, multiple input multiple output

fs is the specified center frequency of the truncated antenna-4 (step-4) and f_d is the frequency of the design step-1.

$$f_d = \frac{f_s}{1.727}. \tag{1}$$

The free space wavelength is $\lambda_d = c/f_d$ where c is the velocity of light, and we can obtain the length of the patch by using Equation (2) where $\lambda_g = \lambda_d/\sqrt{\varepsilon_r}$. To get a better impedance match, the antenna's feed is slightly off by 0.5 mm from the center. Table 1 shows the length of the three antennas with three different specified frequencies.

$$\mathrm{L} = \frac{\lambda_g}{2}. \tag{2}$$

For understanding the design steps, if we take the specified center frequency, f_S, as 9.86 GHz for the design-3, the square patch side in step-1 is L = 12.56 mm. The rectangular patch's upper corner is diagonally truncated in the next step, which is step-2 (antenna-2). Antenna-2 has impedance matching, just reaching −10 dB at 11.25 GHz. In step-3, a lower triangular corner of the antenna-2 is truncated. Lower truncation of the antenna-2 improves further impedance-matching bandwidth, which is now from 8.6 to 11.5 GHz (2.9 GHz). In step-4, a rectangular strip is joined with the ground plane, which further improves the impedance matching band from 8.0 to 11.5 GHz (3.5 GHz) and axial ratio bandwidth (ARBW) from 8.11 to 10.56 GHz (2.45 GHz). Antenna-4 is the final single antenna element (monopole). For the MIMO characteristics, the same antenna is placed firmly like a mirror image on another side of the ground strip, and this is the final step (antenna-5), and it has the same bandwidth as antenna-4.

The proposed two-element MIMO antenna has two monopoles fed by a 50 Ω microstrip line facing each other. These antennas have a common ground plane and are placed nearly with a distance of $0.16\lambda_o$ (5 mm) at f_c = 9.86 GHz. The ground plane strip has been used to enhance the isolation between the antennas and ARBW. The layout and dimensions of the antenna-5 are shown

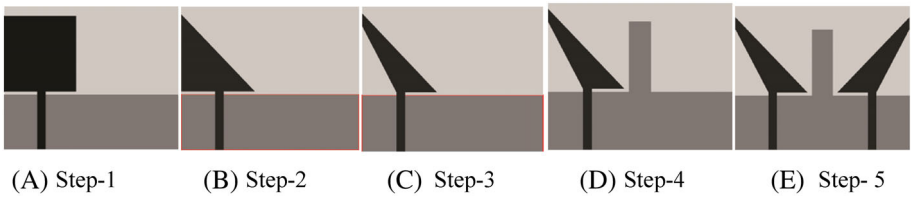

FIGURE 2 Design steps. (A) Step-1. (B) Step-2. (C) Step-3. (D) Step-4. (E) Step-5

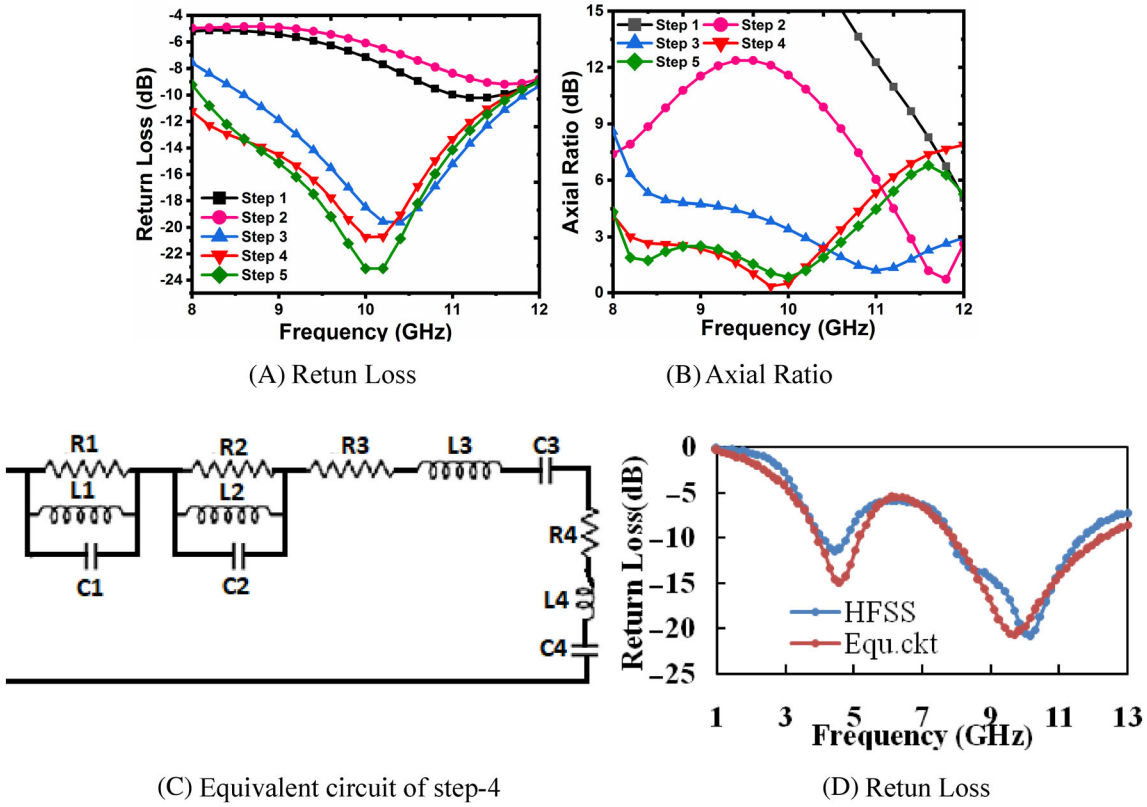

FIGURE 3 Impedance matching, axial ratio band with steps for $f_s = 9.86$ GHz and equivalent circuit of step-4. (A) Retun loss. (B) Axial ratio. (C) Equivalent circuit of step-4. (D) Retun loss

TABLE 1 Length of the square patch (step-1)

Specified frequency (GHz) f_s	Frequency of the design step-1 (GHz) f_d	Length of the patch for step-1 L (mm)	Antenna design
2.0	1.15	62.2	Design-1
5.0	2.895	24.79	Design-2
9.865	5.71	12.56	Design-3

in Figure 1 and which are as follows: $W_s = 29$ mm, $L_s = 23$ mm, $W = 12$ mm, $L = 12.5$ mm, $W_2 = 3.5$ mm, $L_2 = 11$ mm, $L_1 = 9$ mm, $W_f = 1.4$ mm, $L_f = 9.5$ mm, and $L_3 = 10.5$ mm. Strip in the ground plane and lower and upper truncation in the patch provide wide ARBW, pattern and polarization diversity simultaneously. The left-hand side antenna radiates right-hand CP while the right-hand antenna radiates left-hand CP. The antenna performances with systematic design steps of design-3 are illustrated in Figure 3. The impedance matching band improves from step-3 (antenna-3) to step-5 (antenna-5); however, the axial ratio band starts improving from step-2 (antenna-2) to step-5 (antenna-5). Antenna-4 and antenna-5 have wide impedance matching and 3 dB ARBW of 3.52 GHz (8.07–11.59 GHz) and 2.45 GHz (8.11–10.56 GHz), which are shown in Figure 3A,B. Within the impedance matching band, the gain of the antenna is varied from 0 to 3.1 dB.

The equivalent circuit model of the monopole antenna in step-4 is shown in Figure 3C, and its equivalent circuit response is compared with the HFSS model in Figure 3D. The element value of the equivalent circuit are R1 = 880 Ω, L1 = 0.99 nH, C1 = 29.7 pF, R2 = 106 Ω, L2 = 0.67 nH, C2 = 1.02 pF, R3 = 41.9 Ω, L3 = 0.25 nH, C3 = 0.969 pF, R4 = 11.8 Ω, L4 = 0.78 nH, and C4 = 0.9 pF respectively. Figure 4 shows the radiation pattern of the antenna-5 at 8.5, 9.5, and 10.5 GHz. The radiation patterns of antennas are directed in the opposite direction in space, which confirms the pattern diversity. The above-discussed antenna is designed for the specified center frequency $f_S = 9.86$ GHz. The generation of CP in wideband can be understood by analyzing the surface current distribution of step-1, 3, and 4 as illustrated in Figure 5. The dominant component of the surface current on the square patch (step-1) is Jy radiating linear polarized wave, whereas Jx magnitude is minimal, providing cross-polarization. In step-3, a truncated patch enhances the Jx current component. The distribution of the current element Jx is comparatively lesser than the Jy, which generates the

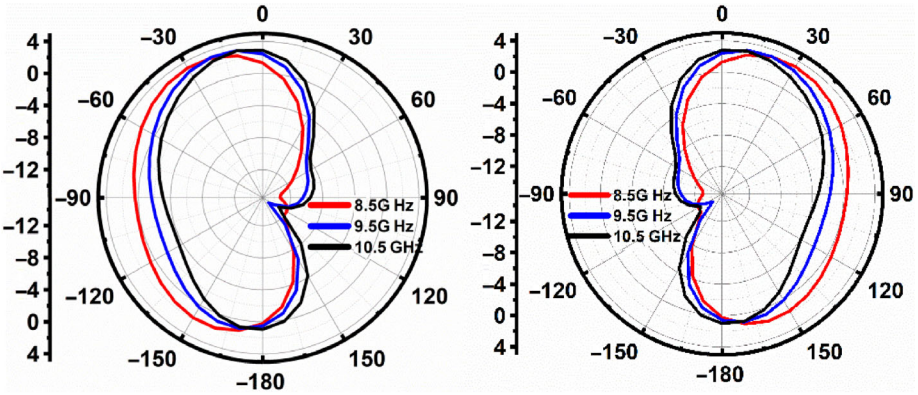

FIGURE 4 Radiation patterns at 8.5, 9.5, and 10.5 GHz showing pattern diversity. (A) Excitation at port-1. (B) Excitation at port-2

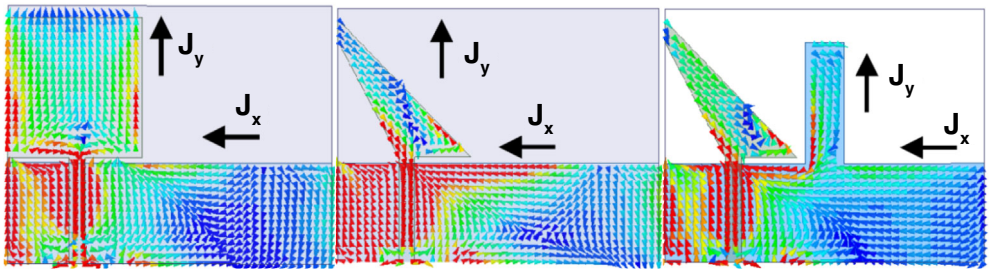

FIGURE 5 Surface current distribution at 8.5 GHz on step-1, 3, and 4. (A) On step-1. (B) On step-3. (C) On step-4

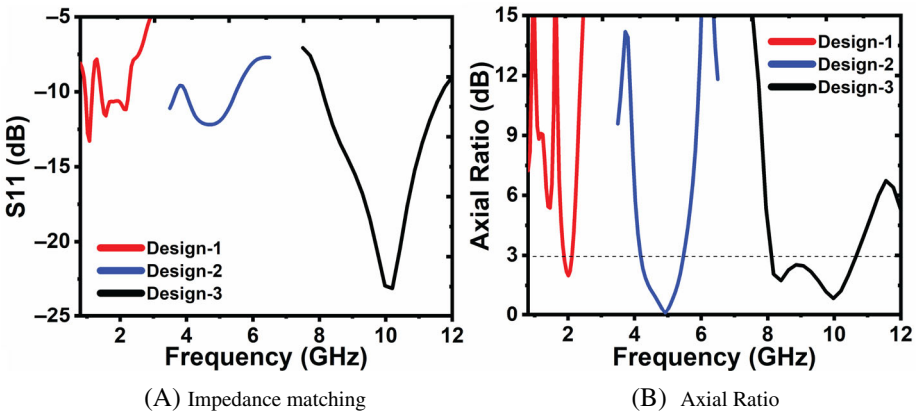

FIGURE 6 Simulated impedance matching and axial ratio with of the design-1, design-2, and design-3. (A) Impedance matching. (B) Axial ratio

elliptical polarization, and its axial ratio dip is lying between 3 and 6 dB. Therefore, to get CP, either we need to increase the magnitude of Jx or decrease the Jy with a phase difference of 90° between them; consequently, we get CP in wideband.

Similarly, to verify the acceptability of Equation (2) for the other frequency bands, we have designed two antennas for two different center frequencies like $f_s = 2$ and 5 GHz, known as design-1 and design-2. The performances of these three antennas (design-1 to design-3) are compared in Figure 6. Figure 6 shows that as the specified center frequency moves downward, the reduction in impedance matching and ARBW starts. Since antenna-3 (design-3) with specified center frequency $f_s = 9.86$ GHz has wider impedance and ARBW than the other designs, we choose this design for the prism and cubical 3D MIMO antennas, which will be discussed in the next sections.

To understand the polarization behavior, we have used surface current distribution and RHCP and LHCP radiation patterns. The surface current on the left-hand side (antenna-A) and right-hand side (antenna-B) antennas, in the X-Y plane with Z, is the direction of propagation. Figure 7A shows the current distribution of port-1 at 8.5 GHz at different phases 0° to 270°. The rotation of the left-hand antenna's surface current is anti-clockwise, and the right-hand antenna surface current rotation is

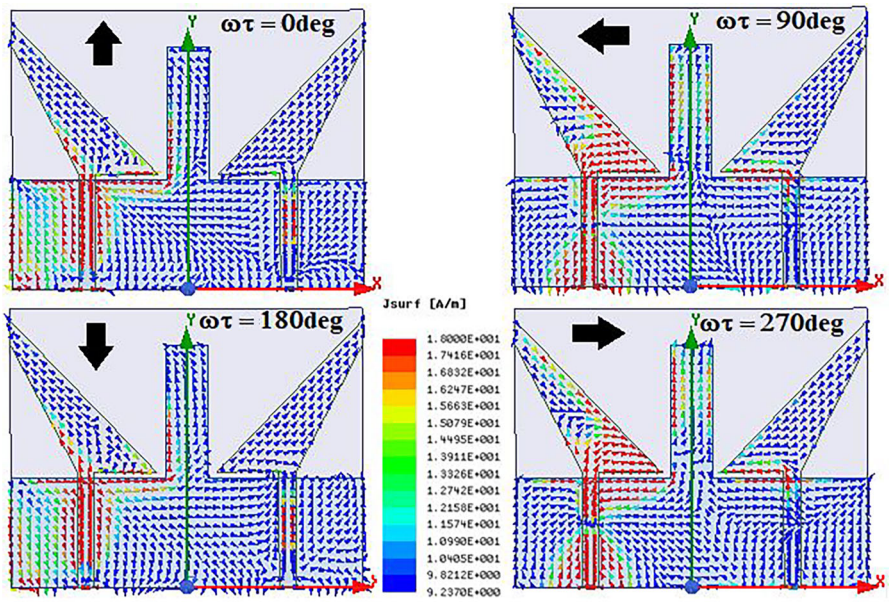

(A) Surface current distribution at 8.5GHz

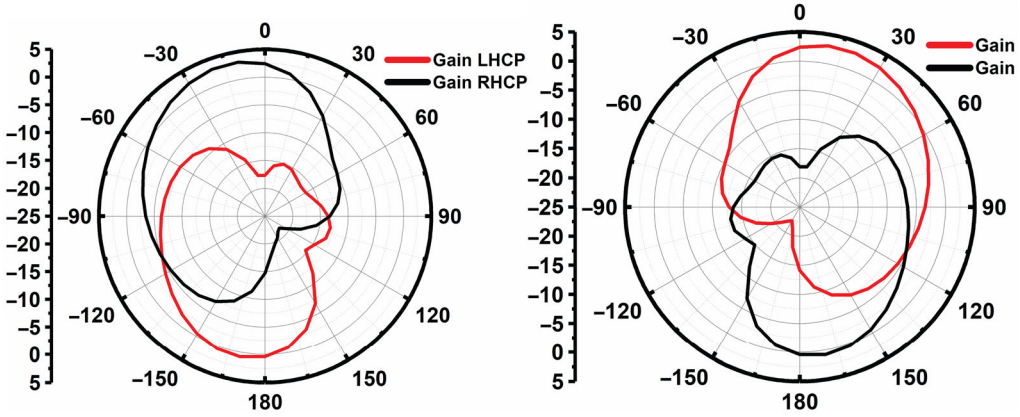

(B) Showing LHCP and RHCP pattern

FIGURE 7 Surface current distribution at 8.5 GHz and LHCP and RHCP pattern. (A) Surface current distribution at 8.5 GHz. (B) Showing LHCP and RHCP pattern

clockwise. Hence, in reference to Z-axis, the left-hand side antenna radiates the RHCP wave while the right-hand side antenna radiates the LHCP wave. The RHCP and LHCP radiation pattern are shown in Figure 7B, showing the pattern diversity in MIMO antennas.

3 | SIX-ELEMENT PRISM MIMO ANTENNA DESIGN

As we know from Equation (3),[33] channel capacity increases as the number of transmitting and receiving antennas increases. In Equation (3), C is the channel capacity in Bits/s, B is the bandwidth in Hz, and M and N are the numbers of transmitting and receiving antennas, and SNR is the signal to noise ratio. To accommodate the multiple numbers of antennas on the user terminal, the terminal size becomes a major limiting factor, and coupling becomes uncontrollable.

$$C = B.W(1 + M \times N \times SNR). \quad (3)$$

The main concern with multiple antenna system designs is that they should be compact, but multiple antennas nearby will increase the mutual coupling between the closely radiated fields. To better understand the MIMO system performance, we propose two 3D MIMO antenna designs systematically. This section will discuss six-elements prism MIMO antenna in detail, while in the next section, eight-elements cubic MIMO antenna will be addressed. The main objective is to place the antennas on prism and cube to get a radiation pattern

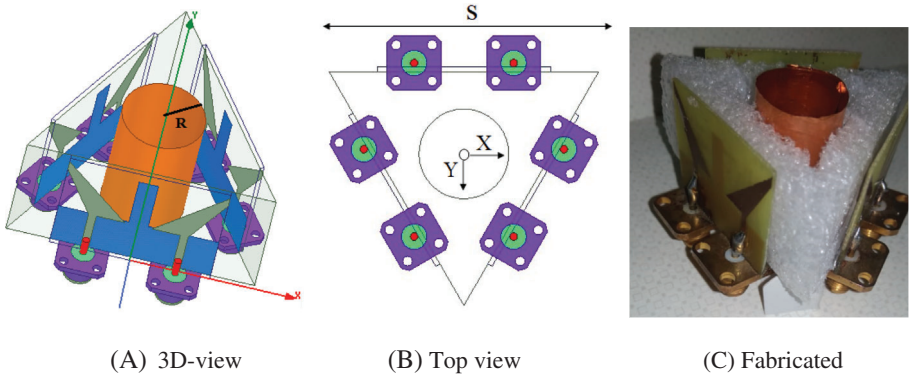

(A) 3D-view (B) Top view (C) Fabricated

FIGURE 8 3D-view of prism shape MIMO antenna. (A) 3D view. (B) Top view. (C) Fabricated. MIMO, multiple input multiple output

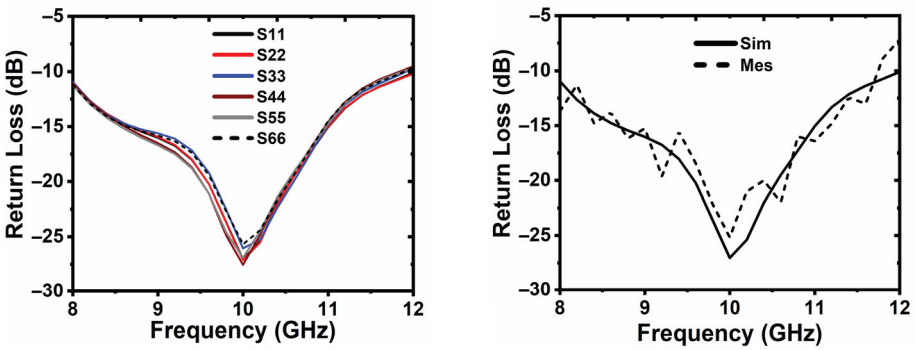

(A) Simulated return loss (B) Measured return loss

FIGURE 9 Simulated and measured return loss. (A) Simulated return loss. (B) Measured return loss

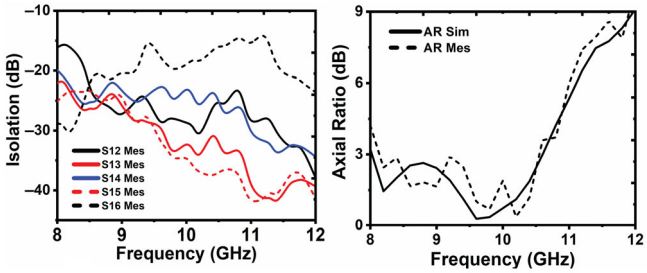

(A) Isolation (B) Axial Ratio

FIGURE 10 Measured isolation and axial ratio. (A) Isolation. (B) Axial ratio

in 360° angular coverage. Prism shaped MIMO antenna of side length S = 45 mm along with fabricated prototype is shown in Figure 8. The two antenna elements are arranged on the face of the prism with an isolating hollow copper cylinder. R is the hollow copper cylinder's radius placed in the middle of the prism to reduce the antenna's mutual coupling. The length of the cylinder is taken the same as the length L_s = 23 mm. Antenna-5, discussed in Section 2 shown in Figure 2E, is arranged clockwise on the prism's face. Each element is radiating in a different direction. The simulated and measured return loss of antennas is shown in Figures 9 and 10.

3.1 | Parametric study

In order to investigate the parametric study of the proposed prism MIMO antenna with a copper cylinder, the radius of the copper cylinder (R) is varied, while other parameters have been fixed. Without a cylinder, the ARBW is reduced, and mutual electric field coupling is high at low frequency. Mutual coupling and ARBW of the prism antennas are the main issues, and it is a big challenge to reduce mutual coupling without disturbing the ARBW. A copper cylinder is being placed inside the prism, which reduces the mutual coupling between the antennas. The proposed antenna is a 3D structure, and it can be seen in Figure 8. Figure 11 shows the prism MIMO antenna's parametric results with a copper cylinder of the radius (R). Without a copper cylinder, the antenna has impedance matching from 8.3 to 11.8 GHz while the isolation in lower frequency is very poor; moreover, the axial ratio band is from 8.7 to 10.5 GHz. As the copper cylinder is being placed inside the prism antenna and increasing its radius, there is an insignificant effect on impedance matching bandwidth (IMBW); however, isolation between the antennas starts improving besides this, the axial ratio band also start improving as shown in Figure 11C.

Figure 11C shows the effect of cylinder radius on the ARBW. ARBW starts improving from R = 6.5 mm to

R = 8.5 mm. After R = 8.5 mm, ARBW starts again deteriorating. Thus, the cylinder radius R = 7.5 mm is selected, giving significantly more ARBW (8.08–10.51 GHz) with improved isolation. Without cylinder, the ARBW is 1.88 GHz, and with cylinder, it becomes 2.45 GHz for radius R = 7.5 mm. This improvement might be due to the metallic cylinder stops affecting the orthogonal components of the adjacent antenna's back lobe radiation. Antennas placement on each face of the prism with copper cylinder provides radiation in a different direction, giving a pattern diversity as shown in Figure 12A. The half-power bandwidth (HPBW) of the antennas are 70° ~ 73° together with covering all 360° angular coverage. The simulated and measured radiation pattern of the prism-shaped MIMO antenna at frequency 9.5 GHz with excitation of port-2 is given in Figure 12B.

4 | EIGHT-ELEMENT CUBICAL MIMO ANTENNA DESIGN

This section discusses the second design of the eight-element cubical MIMO antenna by employing the antenna-5 discussed in Section 2, as shown in Figure 2E. The antenna-5 consists of two monopoles with a mirror

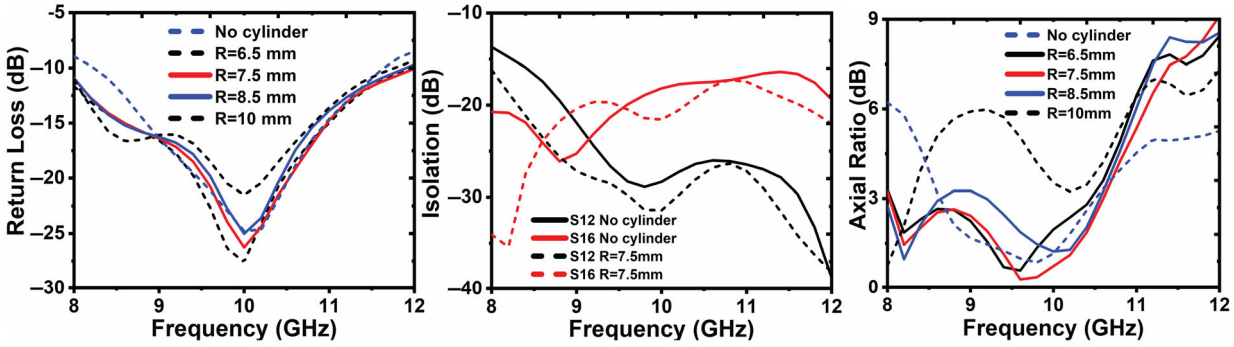

(A) Return loss (B) Isolation (C) Axial Ratio

FIGURE 11 Return loss, isolation, and axial ratio. (A) Return loss. (B) Isolation. (C) Axial ratio

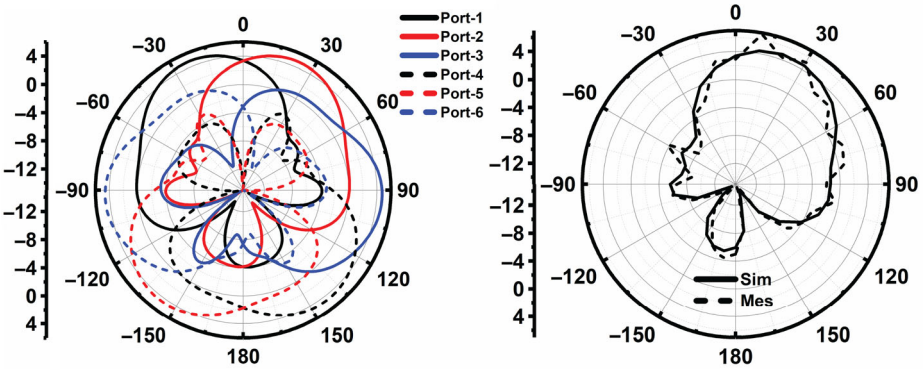

(A) Radiation patterns of multiple ports excitation (B) Measured rad pattern with port-2 excitation

FIGURE 12 Simulated and measured radiation patterns at 9.5 GHz. (A) Radiation patterns of multiple ports excitation. (B) Measured rad pattern with port-2 excitation

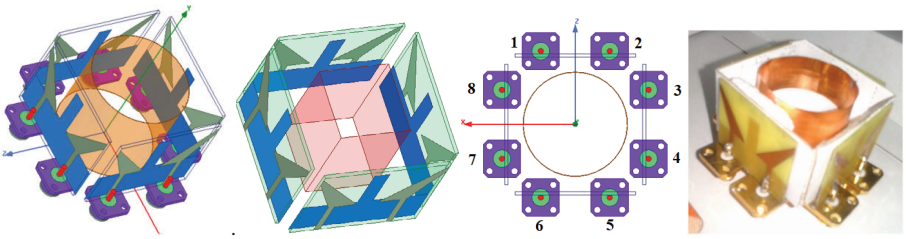

(A) With cylinder (B) With cuboid (C) Bottom view (D) Fabricated prototype

FIGURE 13 The geometry of the proposed eight-element cubic MIMO antenna with copper cylinder and cuboid. (A) With cylinder. (B) With cuboid. (C) Bottom view. (D) Fabricated prototype. MIMO, multiple input multiple output

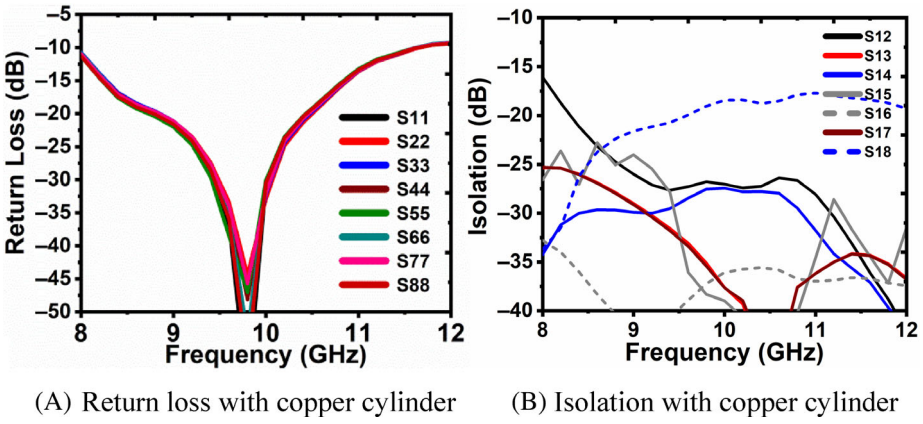

(A) Return loss with copper cylinder (B) Isolation with copper cylinder

FIGURE 14 Simulated response of the proposed cubic MIMO antenna. (A) Return loss with copper cylinder. (B) Isolation with copper cylinder. MIMO, multiple input multiple output

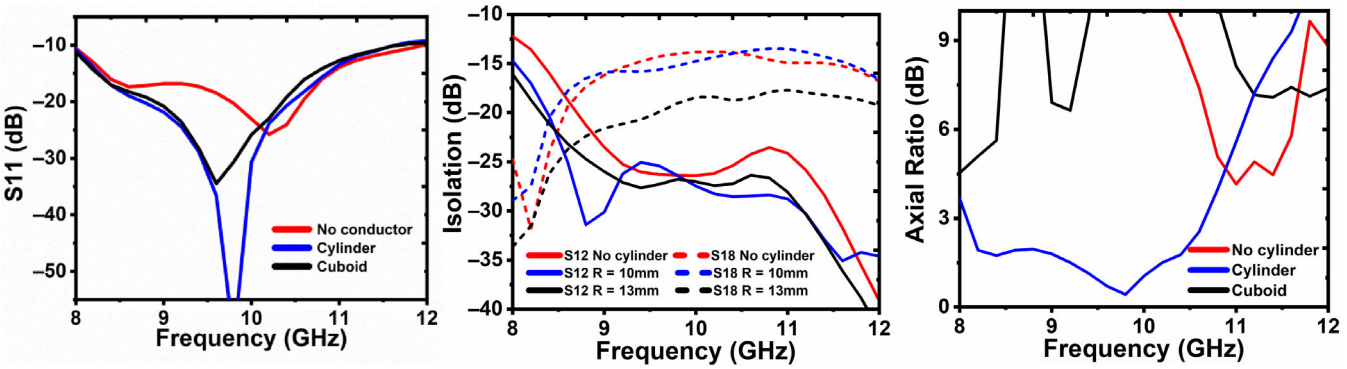

(A) Return loss (B) Isolation (C) Axial ratio

FIGURE 15 Simulated response of the cubic MIMO antenna with and without copper cylinder and cuboid. (A) Return loss. (B) Isolation. (C) Axial ratio. MIMO, multiple input multiple output

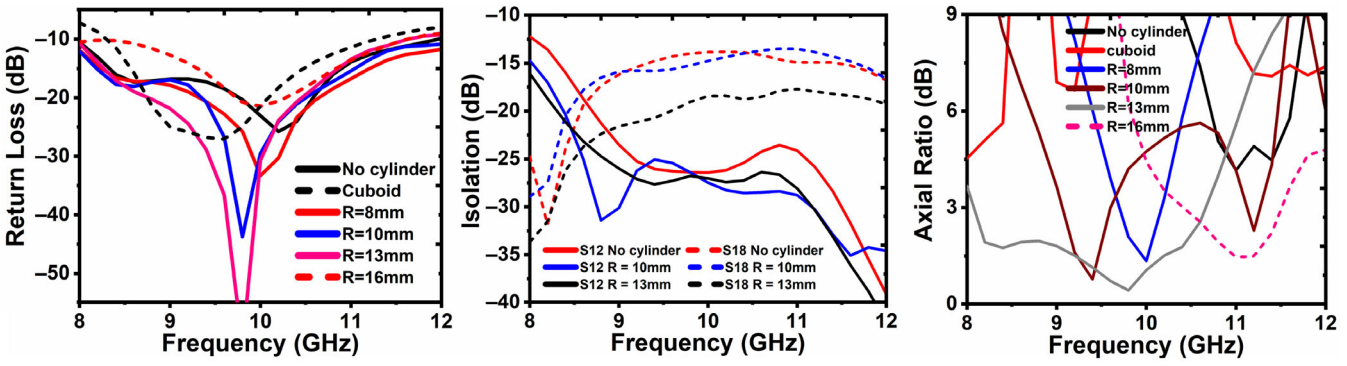

(A) Return loss (B) Isolation (C) Axial Ratio

FIGURE 16 Simulated impedance matching and axial ratio. (A) Return loss. (B) Isolation. (C) Axial ratio

image and facing each other. Moreover, the designed two-element MIMO antenna is in a planar configuration and can be easily arranged in any 3-D configuration with another similar two-elements antenna. For the 3-D structure, four two-element MIMO antennas have been placed on the cube's side faces, as shown in Figure 13. The placement of each antenna is carried out in such a way so that each antenna element radiates in a particular direction.

This work's main objective is to cover the complete 360° angular coverage with a maximum number of antennas embedded in a compact form. Each side face of the cube has two antenna element pairs radiating in the opposite direction. However, as these antennas are

arranged in a compact form and placed closely, the probability of mutual coupling is very high. Two strategies have been used in this work to reduce the mutual coupling between the antennas. In the first one, a hollow copper cylinder is adopted to reduce the mutual coupling, while in another, a hollow copper cuboid is taken. Both the copper cylinder and cuboid are placed at the center of the cube antenna. A copper cylinder with a height (H) and radius "R" is inserted at the middle of the cube to avoid the mutual coupling between antennas.

The height (H) of the copper cylinder and cuboid is the same as the antenna's height ($L_S = 23$ mm). The overall dimension of the proposed cubic MIMO antenna becomes $1.127\lambda_d \times 1.127\lambda_d \times 0.754\lambda_d$ (λ_d is free space wavelength at 9.86 GHz) which consists of a total of eight antennas, and each one is excited by a 50-ohm coax connector. The simulated performances of the proposed cubic MIMO antenna with copper cylinder are shown in Figure 14. However, the result of the cubic MIMO antenna with cuboid is demonstrated in Figure 15. For the sake of brevity, we have just skipped the detailed analysis of the cubic MIMO antenna with cuboid as its performances are not somewhat reasonable compared to the cubic MIMO antenna with the copper cylinder. The performances of the cubic MIMO antenna with copper cylinder and cuboid are compared in Figure 15.

The axial ratio and isolation of the cubic antenna with cuboid are found to be inferior compared to those of

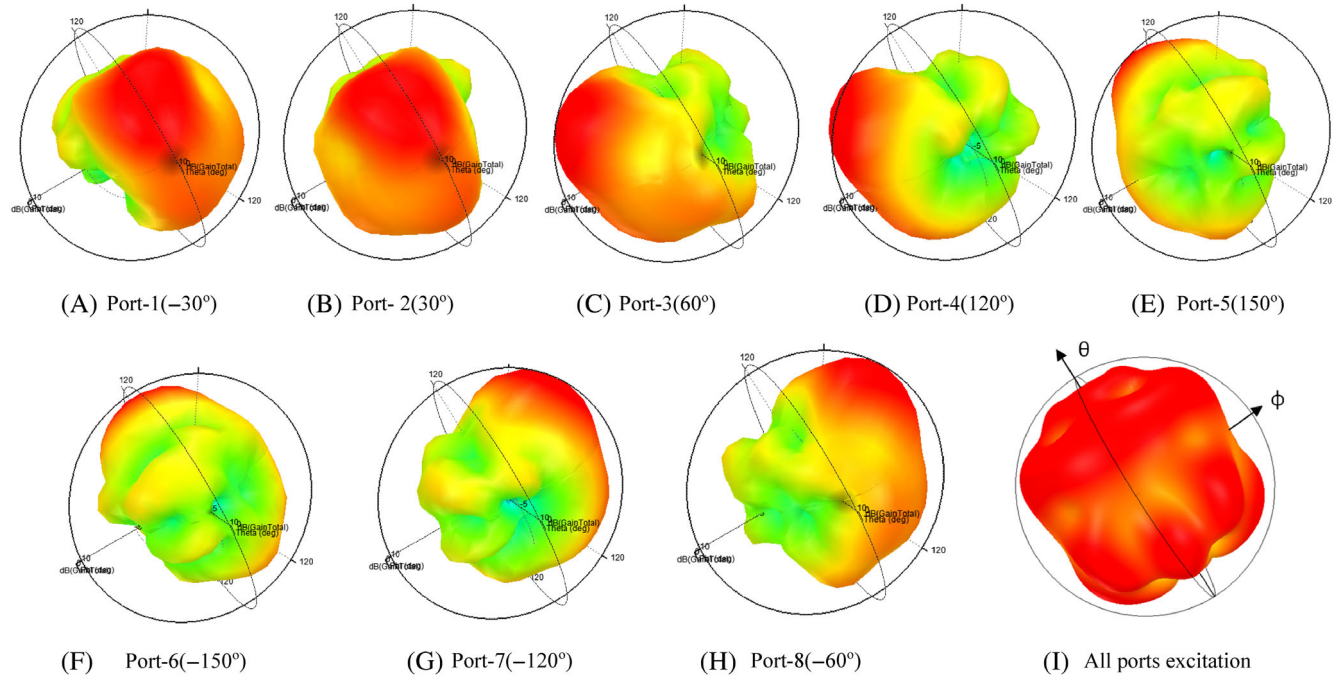

FIGURE 17 Simulated 3D radiation patterns showing pattern diversity at 10 GHz with different port excitation and all port excitation. (A) Port-1 (−30°). (B) Port-2 (30°). (C) Port-3 (60°). (D) Port-4 (120°). (E) Port-5 (150°). (F) Port-6 (−150°). (G) Port-7 (−120°). (H) Port-8 (−60°). (I) All ports excitation

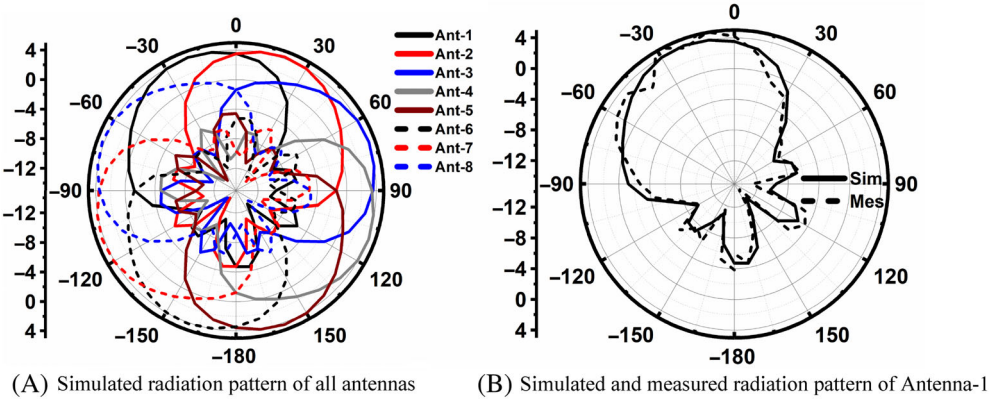

FIGURE 18 The radiation pattern of eight-element cubic massive MIMO antenna at 10 GHz. (A) Simulated radiation pattern of all antennas. (B) Simulated and measured radiation pattern of antenna-1. MIMO, multiple input multiple output

the copper cylinder. Hence, the cubic antenna with copper cylinder has been chosen for further study. The proposed cubic MIMO antenna with the copper cylinder is working in the frequency range of 8.0–12 GHz, with IMBW of 4 GHz, as shown in Figure 15A.In contrast, isolation between antennas is better than −25 dB except between adjacent antennas and between the corner element; it is marginally better than −17.7 dB. In the upper-frequency band, the isolation is somewhat deteriorating; the most probable reason for this is that the fields at edges are highly coupled.

4.1 | Parametric study

In order to investigate the parametric study of the proposed cubic MIMO antenna with a copper cylinder, the radius of the copper cylinder (R) has been chosen, while other parameters have been fixed. Mutual coupling between the antennas in the cube is the main issue, and it is a big challenge to reduce mutual coupling. A copper cylinder is being placed inside the cube, which reduces the mutual coupling between the antennas. The proposed antenna is a 3D structure, and it can be seen in Figure 13. Figure 16 shows the cubic MIMO antenna's parametric results with a copper cylinder radius (R). Without a copper cylinder, the antenna is covering impedance matching from 8.0 to 11.8 GHz while the isolation between the antennas is very poor; moreover, there is no axial ratio band. As the copper cylinder is being placed inside the cubic antenna and increasing its radius, there is an insignificant effect on IMBW; however, isolation between the antennas starts improving besides this, the axial ratio band also start improving as shown in Figure 16C. Isolation between antennas starts improving from −7 to −24 dB as the radius increases from 8 to 13 mm, while 3 dB ARBW starts improving from 1 to 2.69 GHz. At radius R = 14 mm, the isolation and axial ratio start deteriorating. Without cylinder, the axial ratio band is very narrow, from 11 to 11.4 GHz (0.4 GHz). At R = 10 mm, the proposed cubic MIMO antenna gets CP within the dual-band, while for R = 16 mm, the axial ratio band reduces to narrowband with a bandwidth of 0.9 GHz. At R = 13 mm, the proposed cubic MIMO antenna has wide ARBW, which is 2.69 GHz.

5 | RESULTS

The simulated return loss and isolation of the eight-element cubic MIMO antenna are shown in Figure 14A,B. Since the eight-element cubic massive MIMO antenna's essential element is a two-element MIMO antenna, these two element-MIMO antennas have been placed at the cube's four sides to get the radiation pattern in the complete 360° span. The proposed cubic MIMO antenna has covered the full 360° angular coverage with each element's distinct radiation pattern, as shown in the radiation pattern at 10 GHz in Figure 17.The proposed eight-element cubic MIMO antenna has been covering the full angular coverage from 0° to 360° as all antennas are placed on the cube's face. Full angular coverage from 0° to 360° is one of MIMO antenna's essential requirements to handle the situation when pattern loss is probable high in any direction. The 3 dB beamwidth of a single element is 74° ~ 76°, together with all covering the whole 360°.In that scenario, one of the antennas will pick the signal if it is coming from anywhere.

The spatial distribution (angular coverage) property of the MIMO antenna can be understood by employing the 3D radiation pattern, shown in Figure 17. Each one of the antennas is radiating power in a different direction. Antenna-1 (Port-1) radiates in −30°, antenna-2 (Port-2) radiates in 30°, Antenna-3(Port-3) radiates in 60°, and antenna-4 (Port-4) radiates in 120°. Antenna-5 (Port-5) radiates in 150°, antenna-6 (Port-6) radiates in −150° while antenna-7 (Port-7) radiates in -120^0 and antenna-8 (Port-8) radiates in −60° as shown in Figure 17. Figure 17I is showing the radiation pattern of the

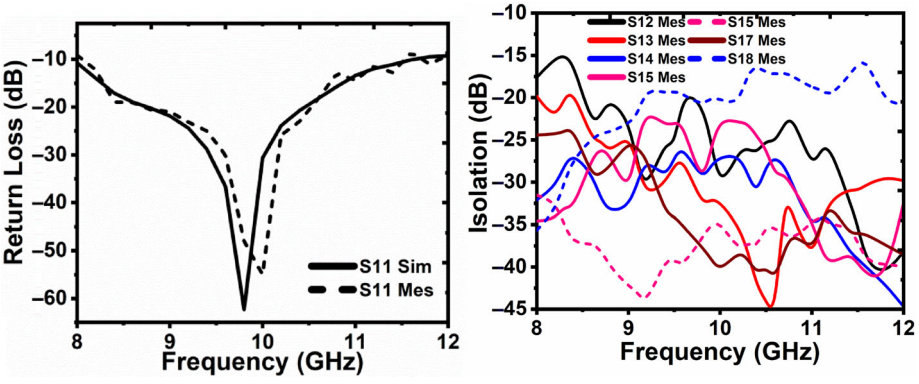

(A) Simulated and measured return loss (B) Measured isolation

FIGURE 19 Simulated and measured results of eight-element MIMO antenna. (A) Simulated and measured return loss. (B) Measured isolation. MIMO, multiple input multiple output

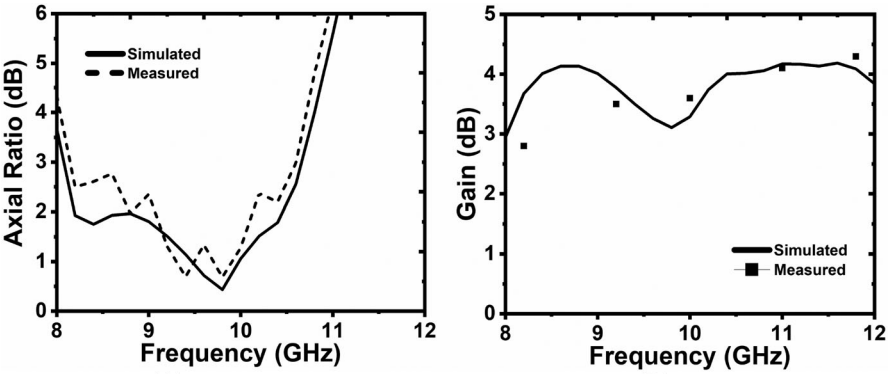

(A) Axial ratio (B) Gain

FIGURE 20 Simulated and measured axial ratio and gain. (A) Axial ratio. (B) Gain

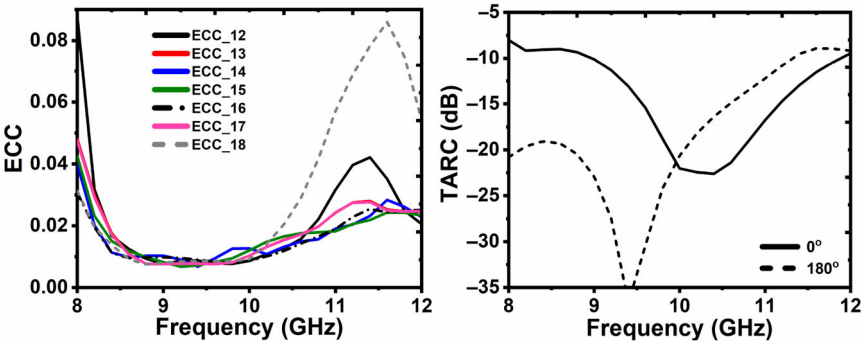

(A) ECC (B) TARC

FIGURE 21 Simulated ECC and TARC of eight-element cubic MIMO antenna. (A) ECC. (B) TARC. ECC, envelope cross-correlation; MIMO, multiple input multiple output; TARC, total active reflection coefficient

antenna by exciting all the ports simultaneously. Figure 18A shows the simulated radiation pattern of the eight-element cubic MIMO antenna at 10 GHz by exciting all the antennas one by one. Figure 18B shows the simulated and measured radiation pattern of a single MIMO antenna element (or exciting a single antenna-3). The measured radiation pattern agrees well with simulated, as shown in Figure 18B.The IMBW is almost the same for all four two-element MIMO antennas as they are placed in symmetry and have a symmetric structure. The proposed antenna is working in the frequency range of 8.0–12 GHz, having IMBW of 4 GHz, as shown in Figure 19A. The isolation between the antenna is better than −25 dB except between antennas 1 and 8, which is slightly worse of −17.5 dB from 10 to 11 GHz and marginally higher at lower frequency region. The measured results of isolation agree well with the simulated results and are shown in Figure 19B. The measured IMBW is 3.4 GHz (8–11.6 GHz), and isolation is better than −20 dB between all the antennas except adjacent antennas. Isolation between adjacent elements antenna-1 and 8, 2 and 3, 4 and 5, 6 and 7 is more significant than −15 dB.

The proposed eight-element antenna has wideband CP with polarization diversity. This type of MIMO antenna is useful when the signal alters polarization after propagation through the free space. In that way, due to multiple reflections, the polarization of the signal becomes uncertain, and the received signal's polarization might not be according to the receiving antenna expectations. In the previous Section 2, the two-element MIMO antenna has polarization diversity. Antenna-1(right-hand side) is radiating RHCP while antenna-2 (left-hand side) radiate LHCP. In cubic MIMO antenna, we have the polarization diversity between the nearby two elements. Thus, in a clockwise direction, one antenna is radiating LHCP, and the other is radiating RHCP and so on.

The antenna's measured ARBW gets slightly deteriorated because of the fabrication tolerance and the presence of some other kind of losses. The measured axial ratio is from 8.13 to 10.52 GHz. Figure 19 shows the simulated and measured axial ratio and gain. The gain of the MIMO antenna varies from 2.8 to 4.3 dB within the entire band. The measured results are reasonably comparable with the simulated results. The probable reason for the deviation of the measured result is the slight copper cylinder misalignment from their axis. The misalignment of the cylinder from the axis disturbs the coupled field distribution among all antennas. Besides this, the copper cylinder reflects the backside field. The cylinder is metallic and reflects the incident wave with 180° out of phase. Hence, the reflected wave combines with the radiated

wave, deteriorating some of the antenna's CP and introducing some polarization losses. (Figure 20)

6 | MIMO PERFORMANCE OF EIGHT-ELEMENT CUBIC MIMO ANTENNA

In order to investigate the performance of the proposed eight-element cubic antenna for MIMO application, the envelope cross-correlation (ECC, $\rho_{e,ij}$) and TARC has been computed by using Equations (4) and (5).[29,31] ECC is the correlation factor that determines how much correlation between the antenna exists. A lower value of ρ_e is desirable. ECC can be calculated by using both far-field and S-parameters. The far-field method involves a more complicated calculation with far-field data, and it is limited to up to 2-element array. In contrast, the ECC measure with S-parameters requires two conditions: first, the antenna should have uniform field distribution, and second, the antenna should be lossless. But practical antennas are lossy and directional to estimate the worst possible case, total radiation efficiencies are considered. This method provides better accuracy when the efficiencies are greater than 60%. In our case, antenna efficiency is greater than 86%. The ECC of all antennas is less than 0.09, shown in Figure 21A.

$$\rho_{ij} = \frac{\left| \sum_{n=1}^{N} S_{ni}^{*} S_{nj} \right|}{\sqrt{\left(1 - \sum_{n=1}^{N} |S_{ni}|^2\right)\left(1 - \sum_{n=1}^{N} |S_{nj}|^2\right)\eta_{rad,i}\eta_{rad,j}} + \sqrt{\left(\frac{1}{\eta_{rad,i}} - 1\right)\left(\frac{1}{\eta_{rad,j}} - 1\right)}}. \quad (4)$$

ECC (ρ_{ij}) is the correlation between the i^{th} and j^{th} elements. The S-parameters S_{ni} and S_{nj} of n port between the i^{th} and j^{th} elements. $\eta_{rad,i}$ and $\eta_{rad,j}$ are radiation efficiencies of i^{th} and j^{th} elements. TARC is defined as the square root of total reflected power to the square root of total incident power. TARC (denoted by Γ_a^t) for any N-element MIMO antenna systems can be obtained from the expression Γ_a^t, given in Reference 31.

$$\Gamma_a^t = \frac{\sqrt{\sum_{i=1}^{N} |b_i|^2}}{\sqrt{\sum_{i=1}^{N} |a_i|^2}}. \quad (5)$$

In the case of 8 × 8 antennas, the scattering matrix can be written as

TABLE 2 Performance comparison with recently published work

Reference	Type	S11 f_L–f_H	IMBW (GHz)	Pattern diversity	Polarization diversity	ARBW (GHz)	Gain (dBi)
12	8 port UWB MIMO	3.1–10.6	7.5	Yes	Linear	NA	2.0–6.8
16	Planar CP MIMO	8.07–11.59	3.47	Yes	Circular	2.45	3–4.8
21	Cavity/slot antenna	5.0–5.4	0.35	Yes	Linear	NA	6.2
22	Slotted cube	5.1–5.3	0.28	Yes	Linear	NA	3.7
24	Cube with magneto-electric dipole	1.77–2.63	1.06	Yes	Linear	NA	1.2, 5.6
26	Slotted cube MIMO	2.8–20.9	18.07	Yes	–	NA	5.9
27	Orthogonally placed	5.6–5.9	0.3	Yes	Linear	NA	4.13–5.83, 2.1–3.51
29	3-D hexagonal structure	3.1–6.2 and 7.1–8.7	3.1, 1.6	Yes	Linear	NA	7.6 ± 1.5
32	3D cuboidal design	3–20	17	No	No	NA	3–6
Our work	Prism shaped	8–11.87	3.87	Yes	Circular	2.43	2.9–4.2
	Cubic shaped	8–11.87	3.87	Yes	Circular	2.69	2.8–4.3

Abbreviations: ARBW, axial ratio bandwidth; CP, circular polarization; IMBW, impedance matching bandwidth; MIMO, multiple input multiple output.

$$\begin{bmatrix} b_1 \\ \vdots \\ b_8 \end{bmatrix} = \begin{bmatrix} s_{11} & \cdots & s_{18} \\ \vdots & \ddots & \vdots \\ s_{81} & \cdots & s_{88} \end{bmatrix} \begin{bmatrix} a_1 \\ \vdots \\ a_8 \end{bmatrix}. \quad (6)$$

Here b_i and a_i represent reflected and incident signals, respectively, which are related to the scattering matrix, S, $b_i = [S]a_j$. Figure 21B shows the frequency variation of simulated TARC (in dB) between the proposed MIMO antennas elements. TARC defines the whole MIMO system's impedance bandwidth for a defined phase angle between the antenna ports. Here, we are considering two cases; in the first case, the phase of all the incidence signals are 0°, while in the second case, it is out of phase. The TARC gets slightly deteriorated at a higher frequency and has insignificant variation at low frequency in the worst case. Table 2 compares the proposed six-element prism and eight-element cube MIMO antenna's performance with the recently published work.[10,21–28] Our proposed six-element prism and eight-element cubic MIMO antennas have better performances compared with the published work.

7 | CONCLUSION

A wideband circularly polarized six-element prism-shaped and eight-element cubic shaped MIMO antennas are designed for the application of X-band (8.0–12 GHz) with both pattern and polarization diversity. Proposed MIMO antennas have pattern diversity with angular coverage within the whole 360°. The isolation between the antennas is better than −25 dB. The IMBW is 4 GHz (8–12 GHz), and the 3 dB ARBW is 2.69 GHz. The envelope correlation coefficient is less than 0.09, and TARC is within the −10 dB within the wide bandwidth. High isolation and uncorrelated radiation patterns between the adjacent elements make the proposed six-element and eight-element antennas a good candidate for use in massive MIMO antenna systems. The size of the antenna is $38.8 \times 38.8 \times 23\ \text{mm}^3$ $(1.127\lambda_d \times 1.127\lambda_d \times 0.754\lambda_d)$. The proposed MIMO antenna could be robust in challenging weather conditions, and it can provide exceptionally high link availability for voice, data, or HD video streaming.

ACKNOWLEDGMENT

Prashant Chaudhary is pleased to acknowledge with thanks the CSIR, Ministry of Human Resource Development, Govt. of India for awarding him the SRF Fellowship to carry out his PhD at Department of Electronic Science, University Delhi, India.

DATA AVAILABILITY STATEMENT

The data that support the findings of this study are available from the corresponding author upon reasonable request.

ORCID

Ashwani Kumar https://orcid.org/0000-0002-7536-6141

REFERENCES

1. Mak CK, Rowell CR, Murch RD. Isolation enhancement between two closely packed antennas. *IEEE Trans Antennas Propag*. 2008;56(11):3411-3419.
2. Zhang S, Ying Z, Xiong J, He S. Ultrawideband MIMO/diversity antennas with a tree-like structure to enhance wideband isolation. *IEEE Antennas Wireless Propag Lett*. 2009;8:1279-1282.
3. Luo S, Li Y, Xia Y, Zhang L. A low mutual coupling antenna array with gain enhancement using metamaterial loading and neutralization line structure. *Aces J*. 2019;34(3):411-418.
4. Li Y, Li W, Yu W. A multi-band/UWB MIMO/diversity antenna with an enhanced isolation using radial stub loaded resonator. *Aces J*. 2013;28(1):8-20.
5. Biswas AK, Chakraborty U. Reduced mutual coupling of compact MIMO antenna designed for WLAN and WiMAX applications. *Int J RF Microwave Comput Aided Eng*. 2018;29:e21629.
6. Jiang T, Jiao T, Li Y. Low mutual coupling MIMO antenna using periodic multi-layered electromagnetic band gap structures. *Aces J*. 2018;33(3):305-311.
7. Saurav K, Mallat NK, Antar YMM. A three-port polarization and pattern diversity ring antenna. *IEEE Antennas Wireless Propag Lett*. 2018;17(7):1324-1328.
8. Roshna TK, Deepak U, Mohanan P. Compact UWB MIMO antenna for tridirectional pattern diversity characteristics. *IET Microwave Antennas Propag*. 2017;11(14):2059-2065.
9. Hu J, Hao Z-C. A compact polarization-reconfigurable and 2-D beam-switchable antenna using the spatial phase shift technique. *IEEE Trans Antennas Propag*. 2018;66(10):4986-4995.
10. Wang J, Shen Z, Zhao L. Wideband dual-polarized antenna for spectrum monitoring systems. *IEEE Antennas Wireless Propag Lett*. 2017;16:2236-2239.
11. Sipal D, Abegaonkar MP, Koul SK. Highly isolated compact planar dual-band antenna with polarization/pattern diversity characteristics for MIMO terminals. *IEEE Antennas Wireless Propag Lett*. 2019;18(4):762-766.
12. Mathur R, Dwari S. 8-port multibeam planar UWB-MIMO antenna with pattern and polarisation diversity. *IEEE Trans Antennas Propag*. 2019;13(3):2297-2302.
13. Mousavi Z, Rezaei P, Rafii V. Single layer CPSSA array with change polarization diversity in broadband application. *Int J RF Microwave Comput Aided Eng*. 2016;27(4):1-8.
14. Luo GQ, Sun LL. A reconfigurable cavity backed antenna for circular polarization diversity. *Int J RF Microwave Comput Aided Eng*. 2016;51(6):1491-1493.
15. Chaudhary P, Kumar A, Yadav A. Pattern diversity MIMO 4G and 5G wideband circularly polarized antenna with integrated LTE band for mobile handset. *Prog Electromagn Res M*. 2020;89:111-120.
16. Chaudhary P, Kumar A, Kanaujia BK. A low-profile wideband circularly polarized MIMO antenna with pattern and polarization diversity. *Int J Microwave Wireless Technol*. 2019;12(4):1-7.

17. Sharma Y, Sarkar D, Saurav K, Srivastava KV. Three element MIMO antenna system with pattern and polarization diversity for WLAN applications. *IEEE Antennas Wireless Propag Lett*. 2016;16:1163-1166.
18. Sipal D, Abegaonkar MP, Koul SK. Compact planar frequency reconfigurable multiple-input multiple-output antenna with pattern and polarization diversity characteristics for WiFi and WiMAX standards. *Int J RF Microwave Comput Aided Eng*. 2020;30:e22121.
19. Li Y, Sim C-Y-D, Luo Y, Yang G. High-isolation 3.5-GHz 8-antenna MIMO array using balanced open slot antenna element for 5G smartphones. *IEEE Trans Antennas Propag*. 2019;67(6):3820-3830.
20. Singh A, Saavedra CE. Wide-bandwidth inverted-F stub fed hybrid loop antenna for 5G sub-6 GHz massive MIMO enabled handsets. *IET Microwave Antennas Propag*. 2020;14(7):677-683.
21. Sun L, Li Y, Zhang Z, Iskander MF. A compact planar omnidirectional MIMO array antenna with pattern phase diversity using folded dipole element. *IEEE Trans Antennas Propag*. 2019;67(3):1688-1696.
22. Sarrazin Y, Mahé Y, Avrillon S, Toutain S. Investigation on cavity/slot antennas for diversity and MIMO systems: the example of a three-port antenna. *IEEE Antennas Wireless Propag Lett*. 2008;7:414-417.
23. Sarrazin J, Mahé Y, Avrillon S, Toutain S. Pattern reconfigurable cubic antenna. *IEEE Trans Antennas Propag*. 2009;54(2):310-317.
24. Chen S, Luk KM. A dual-mode wideband MIMO cube antenna with magneto-electric dipoles. *IEEE Trans Antennas Propag*. 2012;12(12):5951-5959.
25. Getu BN, Andersen JB. The MIMO cube - a compact MIMO antenna. *IEEE Trans Wireless Commun*. 2005;4(3):1136-1141.
26. Yun J. X., Vaughan R.G., "Slot MIMO Cube", Paper presented at: 2010 IEEE Antennas and Propagation Society International Symposium, Toronto, July 2010, pp. 1–4.
27. Jeong JG, Ahn J, Yoon YJ. Ultra-wideband reconfigurable radiation pattern antenna for diversity applications. *Electron Lett*. 2015;52(25):2086-2087.
28. Das G, Sahu NK, Sharma A, Gangwar RK, Sharawi MS. Dielectric resonator based 4-element 8-port MIMO antenna with multi-directional pattern diversity. *IET Microwave, Antennas Propag*. 2019;13(1):16-22.
29. Feng B, Lai J, Zeng Q, Chung KL. A dual-wideband and high gain magneto-electric dipole antenna and its 3D MIMO system with metasurface for 5G/WiMAX/WLAN/X-band applications. *IEEE Access*. 2018;6:33387-33398.
30. Sharawi MS, Hassan AT, Khan MU. Correlation coefficient calculations for MIMO antenna systems: a comparative study. *Int J Microwave Wireless Technol*. 2017;9(10):1991-2004.
31. Manteghi M, Rahmat-Samii Y. Multiport characteristics of a wideband cavity backed annular patch antenna for multi polarization operations. *IEEE Trans Antennas Propag*. 2005;53(1):466-474.
32. Srivastava K, Kanaujia BK, Dwari S, Kumar S, Khan T. 3D cuboidal design MIMO/diversity antenna with band notched characteristics. *Int J Electron Commun (AEÜ)*. 2019;108:141-147.
33. Songs, Shen J. *Evolved Cellular Network Planning and Optimization for UMTS and LTE*. London CRC Press; 2011.

How to cite this article: Chaudhary P, Kumar A, Kumar P, Patel K, Arya RK, Verma AK. 360° angular coverage pattern and polarization diversities wideband circularly polarized multiple input multiple output antennas. *Int J RF Microw Comput Aided Eng*. 2021;e22981. doi:10.1002/mmce.22981